CFD ANALYSIS OF BOILING FLOW IN PWR SUBCHANNEL GEOMETRY OF THE OECD/NRC PSBT BENCHMARK EXERCISE I-1

J. Weis, A. Papukchiev, M. Scheuerer

Gesellschaft für Anlagen und Reaktorsicherheit mbH, Garching, Germany

Abstract

The purpose of the international OECD/NRC PWR Subchannel and Bundle Tests (PSBT) benchmark, based on the NUPEC database, is to provide data for validation of void distribution models. In this paper the RPI wall boiling model, as it is implemented in ANSYS CFX 12.1, is being validated for boiling phenomena in PWR subchannel geometry. In contrast to the original RPI model proposal of Kurul and Podowski [1], the modifications implemented by Egorov and Menter [2] are used to perform the analysis and results are compared to experimental data of PSBT Exercise I-1.

Introduction

One of the most important challenges in nuclear reactor safety analysis is the prediction of critical heat flux (CHF). The critical heat flux depends on flow parameters which can be influenced by the geometrical design of the fuel assemblies, but the development of new fuel assembly components, like the spacer grids, needs expensive experimental campaigns to verify their performance. Therefore it is desirable to combine experimental tests with 3-D thermal-hydraulic calculations or even to replace them by reliable numerical analysis. As a consequence, the development of dependable models for boiling flows is of major interest in reactor safety analysis research.

The first and most well-known sub-grid scale wall boiling model was formulated by Kurul and Podowski [1] from the Rensselaer Polytechnic Institute, which is based on a heat flux partitioning algorithm. In this model, a number of sub-models of the overall mechanistic model were taken from correlations originally developed for application in one-dimensional thermohydraulic simulation methods [3]. Egorov and Menter [2] have formulated modifications of the one-dimensional correlations for application in three dimensional CFD calculations with special attention to achieve mesh independence of the model. The aim of the presented study is to validate the RPI wall boiling model, implemented in ANSYS CFX 12.1, for boiling flow in subchannel geometry against high quality data.

The subchannel void fraction and departure from nucleate boiling data, measured in a representative PWR fuel assembly by the Nuclear Power Engineering Corporation (NUPEC), were identified as one of the most valuable databases for thermal hydraulics modeling. Part of this database is made available for the international benchmark entitled as the NUPEC PWR Subchannel and Bundle Tests (PSBT) benchmark.

In this paper, ANSYS CFX results are presented which were performed for the PSBT Exercise I-1 test cases. Within this study a sensitivity analysis was conducted, evaluating the effects of grid resolution, boundary conditions and modeling approach. The recommendations of the Best Practice Guidelines (BPG) for the use of CFD in Nuclear Reactor Safety (NRS) applications were considered as far as possible [4].

1. PSBT experiments

The PWR Sub-channel and Bundle Tests were conducted by NUPEC within an extensive experimental campaign from 1987 until 1993. Its main objective was to verify the reliability of fuel assemblies used for commercial nuclear power plants [5]. In order to improve the adequacy of fuel and thermal hydraulic design and the safety of nuclear power reactors, PSBT tests reproduced the heat generation in a PWR, in a thermal-hydraulic test facility which can simulate the high-temperature and high-pressure conditions of a real reactor [6][7].

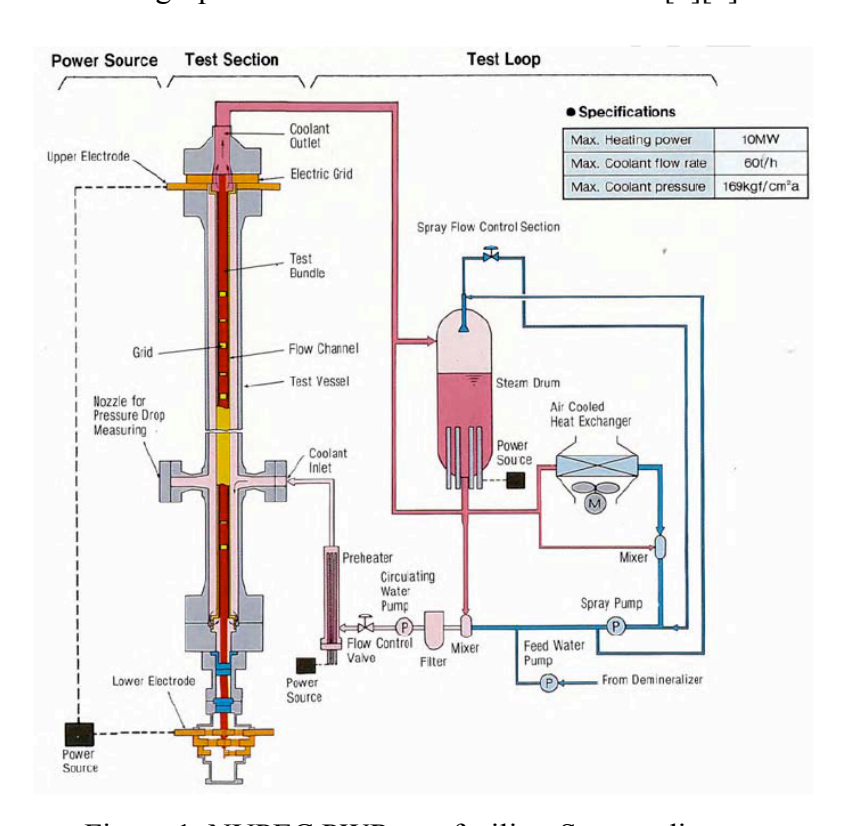


Figure 1: NUPEC PWR test facility: System diagram

As shown in Figure 1 the NUPEC test facility consists of a high pressure and high temperature recirculation loop, a cooling loop, instrumentation and data recording systems. The recirculation loop consists of a test section, circulation pump, pre-heater, steam drum (acting as a pressurizer) and a water mixer [6]. The operating pressure conditions range from 4.9 MPa up to 16.6 MPa, the inlet coolant temperature varies from 140 °C up to 345°C and mass fluxes vary between 550 kg/m²s and 4150 kg/m²s.

1.1 Test section

The void fraction tests of the subchannel experiments were conducted in the test section shown the left side of Figure 2. The coolant inlet nozzle is attached horizontally to the bottom of the test section. At first, the coolant is flowing downward, then it is redirected upward into the subchannel geometry and enters the heated part of the test section. The effective heated length is 1555 mm. The measuring section begins at 1400 mm axial elevation of the beginning of the heated length.

The right side of Figure 2 is showing the four different subchannel geometries of central subchannel, central thimble subchannel (subchannel with one unheated rod), a side and a corner subchannel. The test sections for these 4 different subchannel types were similar. The heaters consist of Inconel 600 and are heated directly. Alumina was used as insulating material and a titanium pipe with a thickness of 4 mm was used as pressure vessel.

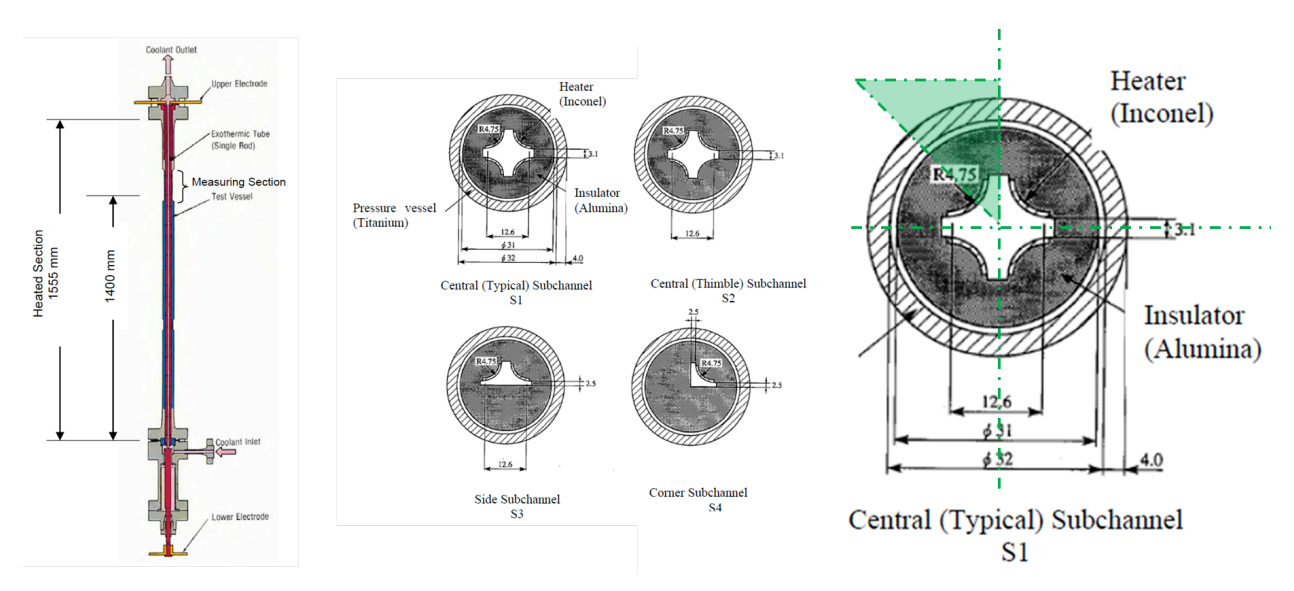


Figure 2: Test Section, 4 different sub-channel geometries and detailed view of central subchannel

1.2 Measurement Procedure

To measure the averaged void fraction within the subchannel cross-section the gamma ray transmission method was adopted. The density of the gas-liquid two-phase flow is measured and converted to the corresponding void fraction. As it is shown in Figure 3 both the narrow gamma-ray beam computed tomography scanner and the wide gamma-ray beam densitometers were used to measure the void fraction in the measuring plane. This procedure was needed to evaluate the relationship between the chordal averaged void fraction and the subchannel averaged void fraction [7]. This relationship was used to obtain the representative void fraction in each subchannel of the rod bundle experiments, which are part of PSBT benchmark exercises I-2 and I-3. The measurement uncertainty of the steady-state void fraction measurement is given in [7] with 3% void, but in discussions within the benchmark community this uncertainty was graded as unrealistic.

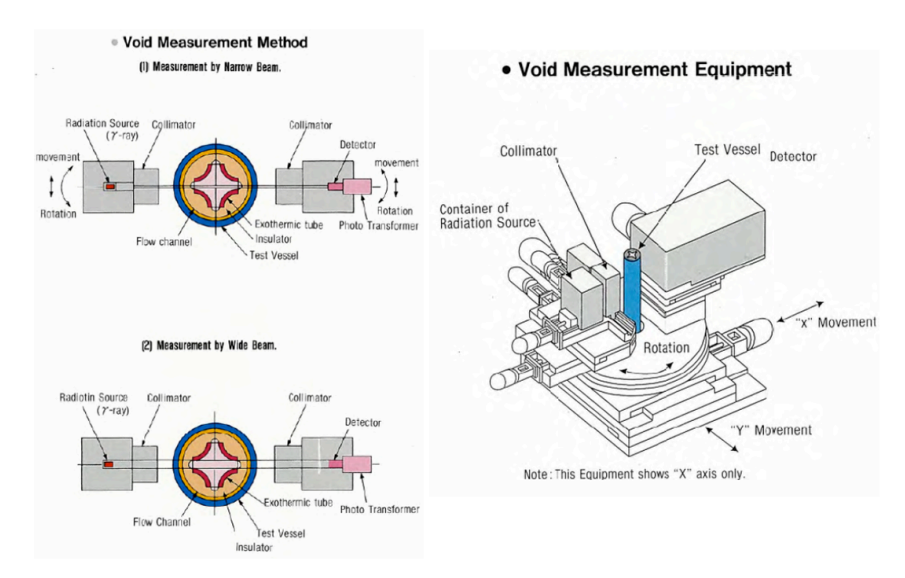


Figure 3: Void fraction measurement method and equipment

1.3 Test matrix

According to final benchmark specifications [7] special test cases were selected to be analyzed as part of benchmark exercise I-1. Table 1 provides an overview of the 16 selected test cases in subchannel geometry S1. For different runs the pressure, the mass flux, the power added to the heater and the inlet temperature of the fluid was varied. The last column gives the subcooling range at the inlet of the test section in different configurations. It ranges from 10.6 K up to 95.7 K.

Table 1: Test conditions of selected runs of steady-state void measurement test series 1

Run No.	Pressure [kg/cm²a]	Mass Flux [10 ⁶ kg/m²h]	Power [kW]	Inlet Temperature [°C]	ΔT _{Sub} [K]
1.1222	169.1	10.98	50.0	334.7	15.6
1.1223	169.1	11.00	49.9	339.7	10.6
1.2211	150.1	10.91	90.0	295.4	45.3
1.2221	150.1	10.88	69.8	299.4	41.3
1.2223	150.1	10.91	69.8	319.6	21.1
1.2237	150.3	10.93	60.0	329.6	11.2
1.2422	150.1	5.00	60.0	284.1	56.6
1.2423	150.3	4.93	59.9	299.3	41.5
1.4311	100.4	5.01	79.9	214.2	95.7
1.4312	100.2	5.03	79.8	248.9	60.8
1.4325	100.3	5.03	59.8	253.8	56.0
1.4326	100.1	5.02	60.1	268.8	40.9
1.5221	75.5	5.02	49.9	219.2	70.4
1.5222	75.0	5.02	50.0	243.9	45.3
1.6221	50.5	5.01	50.0	189.2	74.1
1.6222	50.0	5.00	49.9	204.2	59.5

The subcooling range has a strong influence on the numerical stability of the CFD calculations. With increased subcooling the numerical stability is decreasing as it will be discussed in chapter 2.4.

2. CFD analysis

Due to the large number of test runs which were required within benchmark exercise I-1, the calculations presented in this paper are focused on the subchannel geometry S1. For these test cases symmetry assumptions can be made allowing the use of a simplified model with only one eighth of the geometry, as shown in Figure 2 by the green shaded triangle. A CAD model of this reduced subchannel geometry was created. The length of the subchannel is 1555 mm, corresponding to the heated length in the experiment.

2.1 Initial and boundary conditions

Fully developed velocity profiles as inlet boundary condition were assumed, since no measurements of inlet velocity profiles are available in the NUPEC data. These profiles were calculated by an adiabatic single phase flow calculation with mass fluxes, pressures and temperature conditions according to the experimental test runs. The initial inlet turbulent intensity was derived from the turbulent eddy dissipation and the turbulent kinetic energy of single phase pre-calculations. By giving a mass flow rate as inlet boundary and extracting the resulting velocity field, an error is created depending on the grid resolution. Therefore, the resulting velocity profile was rescaled to the corresponding mass flux. A study was performed checking the accuracy of this approach. It showed that the error can be neglected with the grid resolution of mesh 3 used in the production runs (see chapter 3.3).

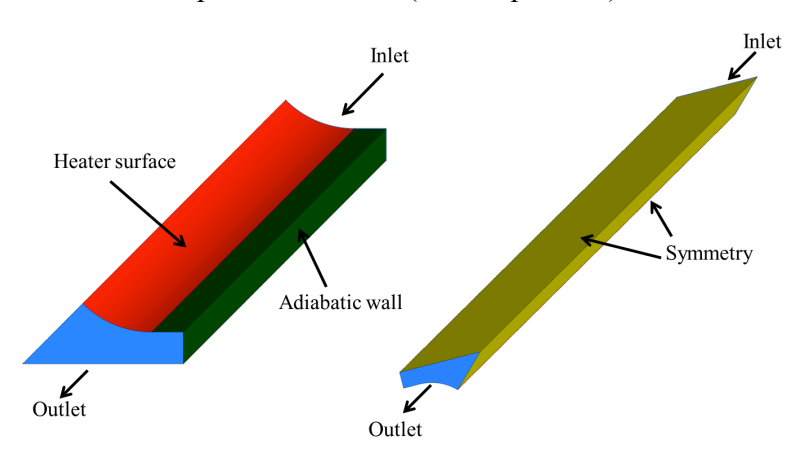


Figure 4: CAD model and boundary conditions

Figure 4 shows the CAD model and the location of the different boundary conditions. The insulated aluminum walls are considered as adiabatic and hydraulically smooth. In case of the heated walls a no-slip boundary condition is chosen for the liquid and a free-slip boundary condition for the gaseous phase. The wall contact model uses the calculated volume fractions to evaluate the wetting of the wall surfaces. As boundary conditions are all steady state, there is only need for transient calculations if convergence of chosen criteria cannot be fulfilled in steady state mode. These transient runs are all initialized by steady state calculations.

2.2 Mathematical models

The two phase flow simulations were defined with water as continuous and steam as dispersed phase. The thermal energy heat transfer model was chosen for the liquid phase and the gas phase was defined to be isothermal at the corresponding saturation temperature. The latter was calculated by a formulation proposed by Wagner et al. [8]. Ishii and Zuber's correlation [9] was used to model the drag force, which is representing the flow resistance.

Concerning the non-drag forces two different set-ups were tested. In the first set up, lubrication forces at the wall and the lift force on the steam bubbles were neglected. Krepper et al. [10] debate the use of a correlation for wall lubrication force for wall boiling cases, because the available models were tested only for adiabatic air water flows. Also, common lift force correlations, like Tomiyama's correlation [11], were derived from air water two phase flow experiments. As a consequence, only the turbulent dispersion force is modeled in the first set-up. It is based on the Favre average of the interfacial drag forces [12]. In the second set-up Tomiyama's lift force correlation [11] was added and Antal's correlation [13] for wall lubrication force (Table 2). Virtual mass forces (or added mass forces) were not modeled in both set-ups.

Table 2: Overview of different set-ups of non-drag forces

Set-up 1	Set-up 2	
Turbulent dispersion force (Favre)	Lift Force (Tomiyama); Wall lubrication force (Antal);	
	Turbulent dispersion force (Favre)	

The RPI wall boiling model as implemented in ANSYS CFX was used for this study. This model divides the heat flux in three partitions: single phase convective heat flux, evaporation heat flux and quenching heat flux. The latter is the heat flux released to the liquid phase during the waiting time after bubble departure. Egorov and Menter [2] implemented several modifications to the RPI model in order to improve its performance. For example, the turbulent heat transfer coefficient in the convective heat flux equation originally using a one-dimensional Stanton number correlation was replaced by a model using the turbulent wall functions. Modifications were also implemented in the formulation of the nucleation site density and the bubble departure diameter, which are the two most important parameters governing the heat partitioning model. In addition, the bubble departure diameter is a function of liquid temperature and to achieve mesh independence a logarithmic form of the wall function with a fixed value of $y^+ = 250$ is used to estimate the liquid subcooling temperature [3]. In this study the maximum vapor area fraction, describing the wall surface area in contact with gas phase was modified from 0.5 to 1 by the user. Two turbulence models were used for the liquid phase, the Shear Stress Transport (SST) model of Menter [14] and a modification of the Reynolds stress model proposed by Launder [15]. The modification of the Reynolds stress model concerns the length-scale equation. In contrast to the original proposal by Launder [8], a version using the turbulent vorticity as length-scale equation was used in this study. Both models were combined with 'automatic' wall functions in which the near-wall fluxes are derived from either linear or logarithmic wall laws, depending on the position of the wall-adjacent grid point. For the gas phase the dispersed phase zero equation model was used. Sato's correlation [16] models the influence of the turbulence transfer, induced by bubble motion on the liquid turbulence.

2.3 Grid generation

Following the OECD/NEA Best Practice Guidelines [4], four hexahedral grids with increasing resolution were generated (Table 3, Figure 5) to perform sensitivity studies. Due to the simple geometry there are no grid angles less than 45°.

Table 3: Overview of different grid resolutions

		Cell size of wall	y ⁺ max	
	Number of cells	adjacent cell	$J = 11x10^6$	$J = 5x10^6$
		adjacent cen	kg/m²h	kg/m²h
Mesh 1	13 x 14 x 150 = 27300	y = 0.1375 mm	335	171
Mesh 2	$16 \times 20 \times 300 = 96000$	y = 0.1100 mm	275	138
Mesh 3	29 x 32 x 500 = 464000	y = 0.0550 mm	139	74
Mesh 4	40 x 43 x 500 = 860000	y = 0.0289 mm	71	41

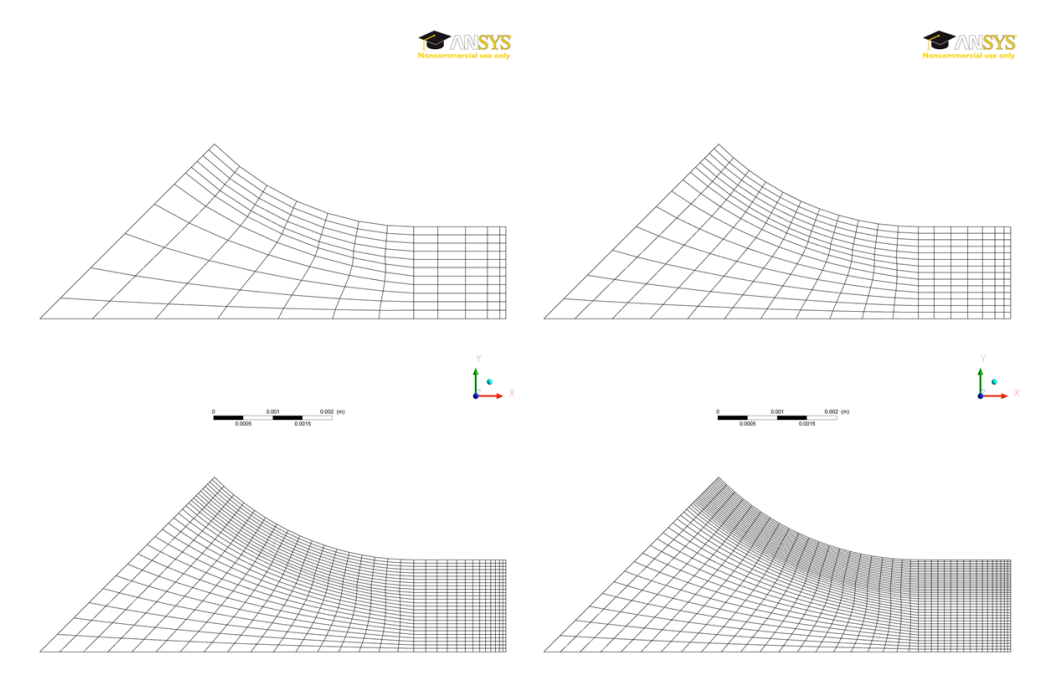


Figure 5: Cross-sectional view of numerical grids

In the first two refinement steps the number of elements was increased in every spatial direction. In the last refinement step from Mesh 3 to 4 special attention was given to the near wall refinement. In contradiction to the recommendations of the BPG for single phase flow, one cannot increase the wall resolution without restrictions, when running a two phase flow boiling simulation with the RPI boiling model. The complete heat flux is distributed to the first cell layer and these elements have to be big enough to absorb the energy by evaporation of the liquid. When using the RPI wall boiling model, it is recommended to use y⁺ values greater than 30. The last columns of Table 3 are showing the y⁺ values of the grids as a function of the two mass flux levels of Table 1.

2.4 Numerical and model errors

As a first step, iteration errors were checked on each grid. In order to economize in computing resources test cases were chosen which converge in steady-state mode. The purpose of this study was to determine a convergence criterion of the iterative CFD solver such that iteration errors became insignificant. Figure 6 shows averaged void fraction, the defined target value for the study, at the outlet of the domain as a function of time steps in an exemplary test case (1.1222). The void fraction did not change any more when the convergence criterion was reduced below 1×10^{-5} RMS. As a consequence, a convergence criterion of 1×10^{-5} RMS was set in the calculations.

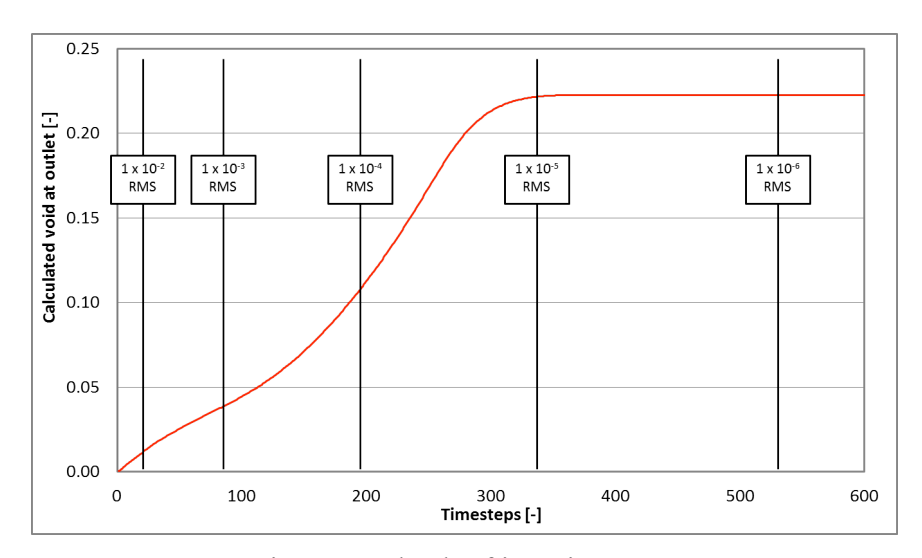


Figure 6: Check of iteration error

This check of iteration error, as it is recommended in BPG, cannot be applied to every test case, because a relationship between the subcooling of the inlet fluid and the convergence behaviour could be observed in the analysis. Test cases with subcooling up to 25 K (cases number 1.1222, 1.1223, 1.223, 1.2237) converged to chosen criteria. Other cases reached a converged solution for the momentum, heat transfer and turbulence equations, but not for the residual of two-phase flow mass imbalance (e.g. test 1.4325). This residual stabilized below 1x10⁻⁴ but never converged to 1x10⁻⁵. Nevertheless, a convergence of integral values could be monitored during the calculations. Cases with higher subcooling needed transient calculations with very small time step sizes (1.0x10⁻³ - 2.5x10⁻⁴ s) to converge. Even in transient mode it was difficult to reach converged solutions for some test cases (e.g. test 1.6222) because the monitored void fraction showed an oscillatory behavior. An explanation can be that the starting point of evaporation is swinging in axial direction during several time steps. In these cases the presented cross-sectional averaged void fractions are the average value of several oscillating periods. As a result, the analysis of the 16 different test conditions (shown in Table 1) is very expensive. Calculation times of test cases with poor convergence exceeded 10 days on 8 parallel processors.

Discretization errors in space are checked by a grid sensitivity analysis and the results are shown in Figure 7. As in the iteration error study, test cases with good convergence were selected in order to save CPU time. The calculated void fraction is varying slightly from mesh 1 to mesh 3. The error difference between the void fractions calculated on mesh 3 and 4 is less than 1%, due to the fact that the radial averaged void fraction is a very insensitive quantity. It was concluded, that this discretization error is small enough and mesh 3 could be used for further calculations.

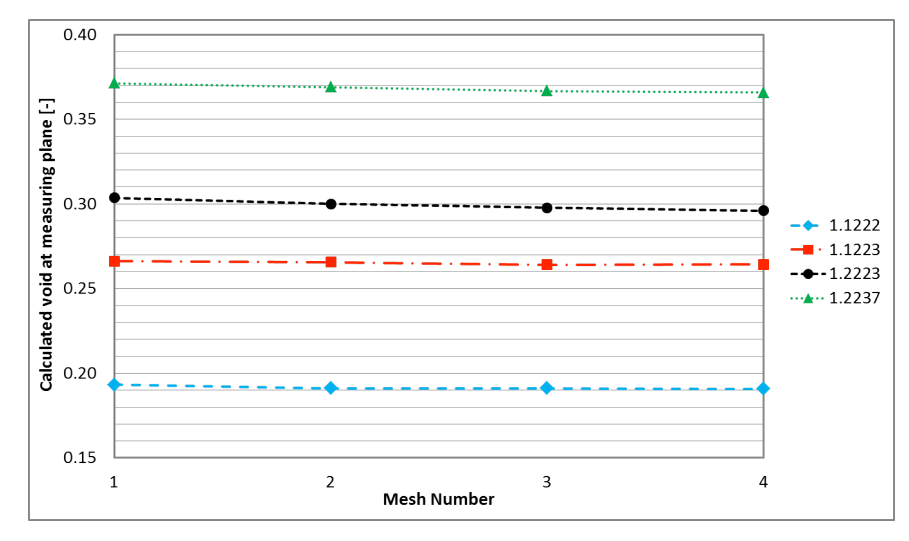


Figure 7: Grid sensitivity analysis

In addition to these observations the numerical stability is decreasing with increased near wall resolution, even though the y^+ values are larger than 30. Due to the acceleration of the fluid along the subchannel length, y^+ is increasing. Therefore the y^+ value can be too small in the regions where evaporation of the fluid becomes the dominant heat transfer mechanism. As a consequence, mesh 3 was chosen for further investigations.

After decreasing the numerical errors, the Baseline Reynolds Stress Model (BSL-RSM) was used instead of Shear Stress Transport (SST) turbulence model, in order to verify the model influence. The main observation was that with BSL-RSM a fully converged solution was even harder to achieve and impossible to reach in steady-state mode. The result of the averaged void fraction did not differ much from the solution with SST model, but the radial distribution of gas bubbles was influenced. Moreover, the results of calculations with BSL-RSM did not satisfy the quality standards of BPG and are therefore not further analyzed.

3. CFD results and comparison to experimental data

Finally, the results are compared to experimental data. Figure 8 shows the calculated void fraction of the 16 test cases of Table 1 with the SST turbulence model and the first set-up for non-drag forces. The black line would be the perfect agreement between calculation and experiment. The dashed lines are showing \pm 5% uncertainty borders of the experiment. In general, the results are in good agreement with experimental data and within the experimental error range. Notable is the fact that test cases with void fractions above 30% are calculated satisfactorily although the RPI wall boiling model is developed for subcooled boiling and the steam temperature is limited to saturation conditions in this study. In addition, no influence of the pressure level on the results could be observed.

The comparison of the two different set-ups for non-drag forces (see chapter 2.2) showed a slight improvement after adding correlations for lift and wall lubrication force, as shown in Figure 9. Due to poor convergence performance only selected test cases were calculated with this second set-up.

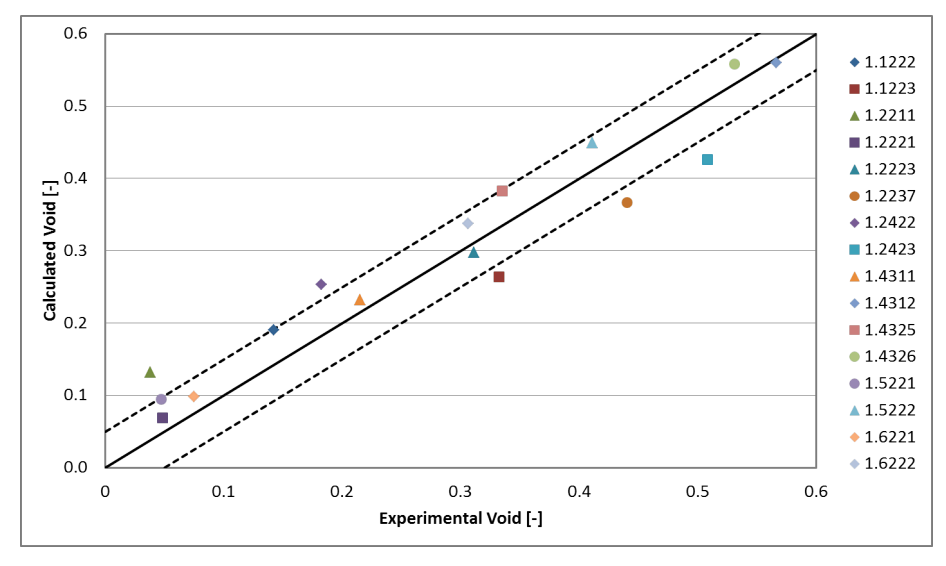


Figure 8: Comparison to experimental data: listed by run-no.

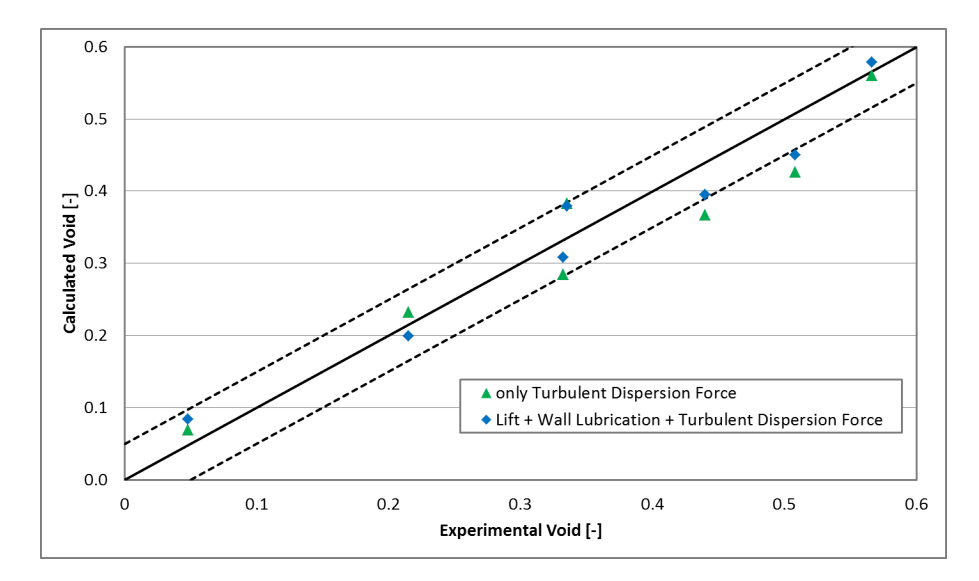


Figure 9: Comparison between set-up 1 and 2 of non-drag forces

Figure 10 demonstrates the influence of the added lift force and wall lubrication force on the distribution of gas bubbles. The presented test case is \$1.1223. The calculated, averaged void fractions are 0.284 for set-up 1, 0.308 for set-up 2. The average value 0.332 is derived from the experimental measurement. In Figure 10, the maximum void fraction was set to 60% to increase the color contrast in the simulation pictures. With set-up 1 the gas bubbles are distributed nearly uniformly in radial direction. In contrast, the solution shown for set-up 2 has no steam in the center of the subchannel and a high bubble concentration at the heated wall. The experimental CT-scan shows, besides some spots of high void fractions, an almost homogenous distribution. Figure 11 presents the void distribution of test case \$1.2423. The solution of set-up 2 is showing an accumulation of gas bubbles in unheated corners of the subchannel, which is in good agreement with the CT-scan. The averaged void fractions are 0.426, 0.460 and 0.508 respectively. In conclusion it cannot be stated that including correlations for lift and wall lubrication force improved the agreement of void distribution with experimental observations.

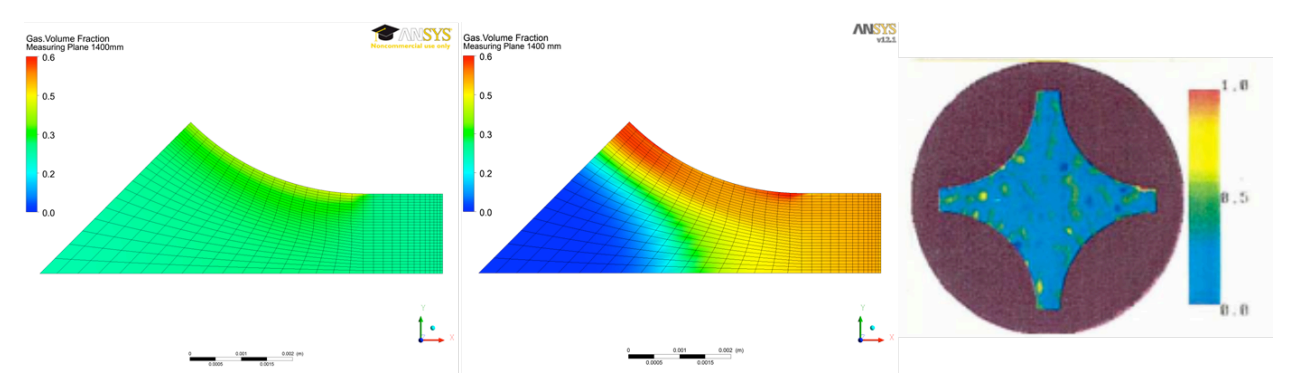


Figure 10: Void distribution: set-up 1, set-up 2, experimental CT-scan (S1.1223)

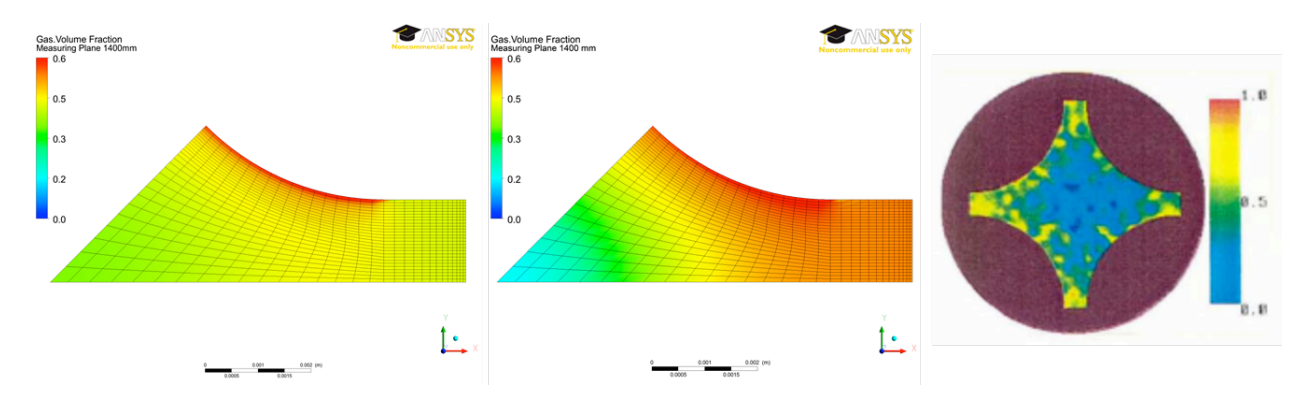


Figure 11: Void distribution: set-up 1, set-up 2, experimental CT-scan (S1.2423)

4. Conclusion

A numerical analysis of the PSBT Benchmark Exercise I-1 was performed with the CFD software ANSYS CFX 12.1. The results were compared with averaged void fractions at the measurement section. The goal was to validate the RPI wall boiling model against benchmark data. The numerical grid generation and error analysis was performed according to the OECD Best Practice Guidelines. An effort was made to establish convergence criteria which reduce iteration and discretisation errors for the different test cases to an acceptable value. After minimizing the numerical errors, model errors were investigated by comparing different turbulence models and set-ups for the boiling models. The final comparison with data showed good agreement for the cross-sectional averaged void fractions. Further investigations are planned to examine the influence on non-drag forces on radial distribution of gas bubbles and bubble departure diameter on void fractions.

Acknowledgements

This work has been funded by the German Federal Ministry of Economics and Technology within reactor safety research project RS 1184.

5. References

- [1] N. Kurul, M.Z. Podowski, "On the modeling of multidimensional effects in boiling channels", <u>ANS Proc. 27th National Heat Transfer Conference</u>, Minneapolis, MN, July 1991.
- [2] Y. Egorov, F. R. Menter, "Experimental implementation of the RPI boiling model in CFX-5.6", Technical Report ANSYS/TR-04-10, 2004.
- [3] ANSYS CFX Solver Theory Guide, ANSYS CFX Release 12.1, 2009.
- [4] J. Mahaffy et al., "Best practice guidelines for the use of CFD in nuclear reactor safety applications", NES/CSNI/R(2007)5, April 2007.
- [5] K. Hori et al., "In Bundle Void Fraction Measurement of PWR Fuel Assembly", <u>ICONE-2</u>, Vol. 1, San Francisco, California, March 1993.
- [6] M. C. Galassi et al., "Validation of NEPTUNE_CFD against PSBT experimental tests", NURISP D-2.2.2.10, June 2010.
- [7] A. Rubin et al., "OECD/NRC Benchmark based on NUPEC PWR Subchannel and Bundle Tests (PSBT), Volume I: Experimental Database and Final Problem Specifications", NEA/NSC/DOC(2010)1, November 2010.
- [8] W. Wagner, H.-J. Kretzschmar, "International Steam Tables: Properties of Water and Steam based on the Industrial Formulation IAPWS-IF97", Springer-Verlag, Berlin 1998.
- [9] M. Ishii, N. Zuber, "Drag coefficient and relative velocity in bubbly, droplet or particulate flows", AlChE J. 25, 1979.
- [10] E. Krepper, B. Končar, Y. Egorov, "CFD modelling of subcooled boiling Concept, validation and application to fuel assembly design", Nuclear Engineering and Design, Vol 237, April 2007, pp. 716-731.
- [11] A. Tomiyama, "Struggle with computational bubble dynamics", <u>Third International Conference on Multiphase Flow</u>, Lyon, France, June 1998.
- [12] A.D. Burns et al., "The favre averaged drag model for turbulence dispersion in Eulerian multi-phase flows", 5th Int.- Conf. on Multiphase Flow, Yokohama, Japan 2004.
- [13] S.P. Antal et al., "Analysis of phase distribution in fully developed laminar bubbly two-phase flow", Int. J. Multiphase Flow 7, 1991.
- [14] F. R. Menter, "Two-Equation Eddy-Viscosity Turbulence Models for Engineering Applications", AIAA-Journal, Vol. 32, pp. 269 289, 1994.
- [15] B. E. Launder et al., "Progress in the development of a Reynolds stress turbulence closure", J. Fluid Mech. 68:537-66, 1975.
- [16] Y. Sato et al., "Momentum and heat transfer in two-phase bubble flow", Int. J. of Multiphase Flow 7, 1981.